Nanoscale

PAPER

View Article Online
View Journal | View Issue

Cite this: *Nanoscale*, 2024, **16**, 14748

A multifunctional protein pre-coated metal–organic framework for targeted delivery with deep tissue penetration†

Jun Yong Oh,‡ Min-Seok Seu,‡ Ayan Kumar Barui, ‡§ Hae Won Ok, Dohyun Kim, Eunshil Choi, Junmo Seong, Myoung Soo Lah and Ja-Hyoung Ryu *

Targeted drug delivery using metal–organic frameworks (MOFs) has shown significant progress. However, the tumor microenvironment (TME) impedes efficient MOF particle transfer into tumor cells. To tackle this issue, we pre-coated nano-sized MOF-808 particles with multifunctional proteins: glutathione S-transferase (GST)-affibody (Afb) and collagenase, aiming to navigate the TME more effectively. The surface of MOF-808 particles is coated with GST-Afb—a fusion protein of GST and human epidermal growth factor receptor 2 (HER2) Afb or epidermal growth factor receptor (EGFR) Afb which has target affinity. We also added collagenase enzymes capable of breaking down collagen in the extracellular matrix (ECM) through supramolecular conjugation, all without chemical modification. By stabilizing these proteins on the surface, GST-Afb mitigate biomolecule absorption, facilitating specific tumor cell targeting. Simultaneously, collagenase degrades the ECM in the TME, enabling deep tissue penetration of MOF particles. Our resulting system, termed collagenase-GST-Afb-MOF-808 (Col-Afb-M808), minimizes undesired interactions between MOF particles and external biological proteins. It not only induces cell death through Afb-mediated cell-specific targeting, but also showcases advanced cellular internalization in 3D multicellular spheroid cancer models, with effective deep tissue penetration. The therapeutic efficacy of Col-Afb-M808 was further assessed *via in vivo* imaging and evaluation of tumor inhibition following injection of IR-780 loaded Col-Afb-M808 in 4T1tumor-bearing nude mice. This study offers key insights into the regulation of the multifunctional protein-adhesive surface of MOF particles, paving the way for the designing even more effective targeted drug delivery systems with nano-sized MOF particles.

Received 5th June 2024,
Accepted 17th June 2024

DOI: 10.1039/d4nr02345e

rsc.li/nanoscale

Introduction

Nano-sized metal–organic framework (MOF) particles have emerged as a cutting-edge choice in the field of drug delivery.[1–4] These materials, synthesized by assembling metal ions/clusters and organic ligands, form porous coordination polymers.[5–7] Notably, Zr-based metal–organic frameworks (MOFs) have garnered significant attention due to their remarkable stability in water.[8–10] These species consist of Zr_6 clusters that can interconnect in up to 12 directions.[11] Moreover, the unsaturated sites, determined by the connectivity of the Zr_6 cluster, enable facile exchange with other coordinating substances.[12] This characteristic opens up avenues for acquiring new functional properties, including the incorporation of targeting ligands.[13,14] In our previous studies, we proposed creating a protective shield using supramolecular conjugation between MOF and a recombinant protein.[15] This protein is fused with targetable affibodies (Afbs) such as the glutathione S-transferase (GST)-human epidermal growth factor receptor 2 (HER2) or epidermal growth factor receptor (EGFR) affibody (Afb), referred to as GST-Afb.[16,17] By modulating the reactive surface properties of MOF particles, this protective shield effectively mitigates the protein corona phenomenon enveloping the nanoparticle.[18–22] This, in turn, enhances the performance of drug delivery systems (DDS) based on MOF nanoparticles. Despite these endeavors, gaining a comprehensive understanding of particle behavior within the tumor microenvironment (TME) remains crucial.[23–25] The extracellular matrix (ECM), for instance, forms an intricate network of proteins and carbohydrates enveloping cells in various tissues and organs.[26] Acting as a formidable physical barrier, the ECM poses challenges to the efficient penetration and distribution of therapeutic agents in tissues.[27] Consequently, it can curtail

Department of Chemistry, Ulsan National Institute of Science and Technology, Ulsan 44919, Republic of Korea. E-mail: jhryu@unist.ac.kr

† Electronic supplementary information (ESI) available. See DOI: https://doi.org/10.1039/d4nr02345e

‡ These authors are equally contributed.

§ Present address: Department of Biomedical and Pharmaceutical Sciences, Harry and Diane Rinker Health Science Campus, Chapman University, 9401 Jeronimo Road, Irvine, CA 92618-1908, USA.

drug bioavailability, diminish efficacy, and hinder precise targeting of specific cells or disease sites.[28] Therefore, it is imperative to devise strategies that enable effective traversal of the ECM and enhance drug delivery, underscoring their paramount significance.

In this study, we introduce a novel approach that involves pre-coating and functionalizing the reactive surface of MOF-808 particles with multifunctional proteins (GST-Afb and collagenase) for targeted cancer treatment and ECM degradation (Fig. 1). The reactive surface of MOFs is capable of coordinative interactions with the carboxylate groups that found in proteins.[29–33] This allows for direct supramolecular conjugation between the proteins and MOF-808 particles, eliminating the need for specialized chemical linkers. As a result, a stable and functional protein layer is formed on the surface of MOF-808 particles. The collagenase-GST-Afb-MOF-808 system, hereinafter referred to as Col-Afb-M808, comprises a functional protein layer. This layer showcases cell-specific targeting capabilities, particularly towards HER2-overexpressing cancer cells like SK-BR-3. Moreover, it provides a shielding effect, mitigating the protein corona phenomenon typically seen in biologically simulated environments. The system also incorporates surface collagenase, which accelerates the degradation of the ECM in a 3D multicellular spheroid cancer model. This feature enables superior deep tissue penetration. Moreover, cellular experiments have validated that the co-application of functional proteins on the particle surface elicits a more pronounced synergistic effect compared to their individual application. The therapeutic efficacy of Col-Afb-M808 was further confirmed by employing 4T1 tumor-bearing nude mice that were treated with IR-780-loaded Col-Afb-M808. This approach presents a valuable strategy for controlling the interfaces between nano-sized Zr-MOF particles and proteins, paving the way for future applications in targeted drug delivery systems.

Methods

Benzene-1,3,5-tricarboxylic acid (BTC) (95%), zirconyl chloride octahydrate ($ZrOCl_2{\cdot}8H_2O$) (reagent grade, 98%), formic acid (ACS reagent, ≥96%), acetic acid (ACS reagent, ≥99.7%), difluoroacetic acid (98%), collagenase, fluorescein isothiocyanate, and dimethyl sulfoxide were purchased from Sigma-Aldrich. Acetone (≥99.5% (m m^{-1})), methanol (≥99.5% (m m^{-1})), and *N*,*N*-dimethylformamide (DMF) (≥99.5% (m m^{-1})) were purchased from Junsei. 1,1′-Dioctadecyl-3,3,3′,3′-tetramethylindocarbocyanine perchlorate (DiI), 1× PBS without calcium or magnesium, BCA assay kit, and EnzChek™ Gelatinase/Collagenase Assay Kit were purchased from Thermo fisher. CD44 antibody was purchased from BioLegend. Deionized (DI) water was produced by the Millipore Milli-Q system (18.2 MΩ cm). SK-BR-3, and 4T1 cells were purchased from the Korean cell line bank (KCLB catalog no. 30030).

Preparation of MOF-808

MOF-808 was prepared following a reported procedure.[14,34] In a 50 mL Pyrex vial, 0.3 mmol of $ZrOCl_2{\cdot}8H_2O$, and 0.4 mmol of BTC were dissolved in a mixture of 5 mL DMF and 5 mL formic acid. The solution was then placed in an oven at 100 °C for 18 h. The resulting white precipitate was washed first with

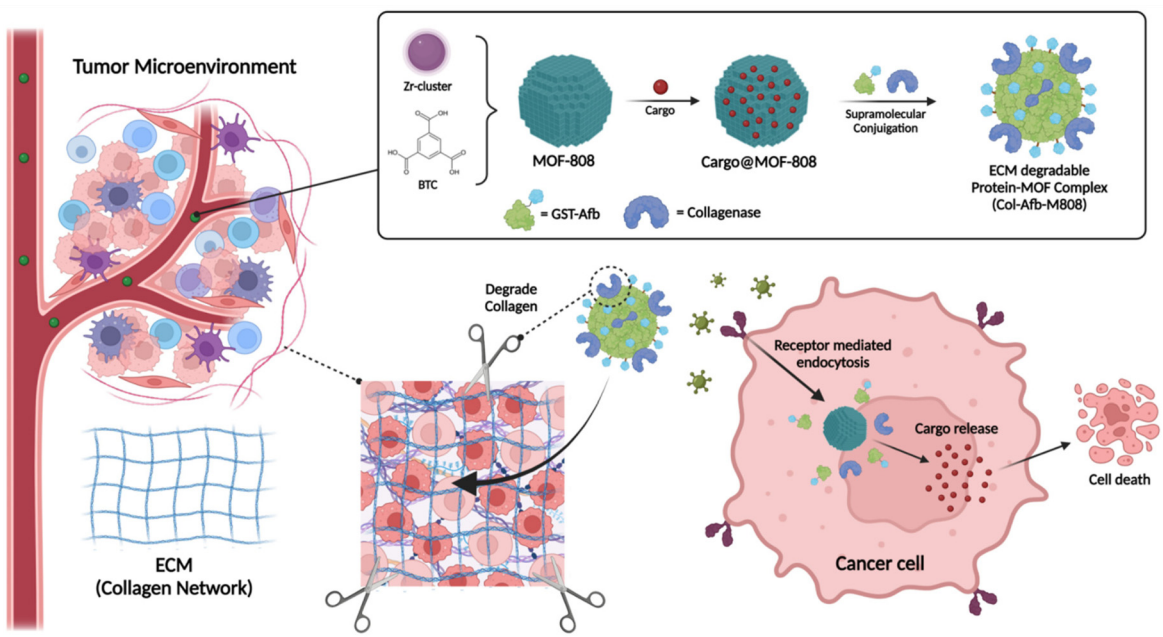

Fig. 1 Schematic depiction of multifunctional pre-coated MOF-808 nanoparticles (Col-Afb-M808) for effective targeted nanomedicine. The surface of the MOF-808 nanoparticles is precoated with GST-Afb, which serves both as a protective shield and a targeting moiety. Additionally, collagenase acts as an ECM-degradable enzyme, promoting deep tissue penetration. The therapeutic synergistic effects of the MOF particles are achieved by the chemotherapeutic drug preloaded inside them.

DMF and subsequently with methanol (MeOH). The obtained MOF-808 particles were then immersed in MeOH for preparation for the protein attachment experiment. They were activated at room temperature for 12 h and subsequently heated at 150 °C for another 12 h under vacuum before further use.

Preparation of Col-M808 or Afb-M808

0.5 mg of MOF-808 particles were mixed and stirred with 0.4 mg of collagenase or 0.4 mg of GST-Afb in 2 mL of neutral PBS.[16] The mixture was stirred for 30 min at 4 °C and then centrifuged at 3220*g* using an Eppendorf Centrifuge 5415R to remove unreacted free proteins. The obtained Col-M808 or H-M808 particles were washed with water and re-dispersed in PBS.

Preparation of Col-Afb-M808

0.5 mg of MOF-808 particles were mixed and stirred with 0.2 mg of collagenase and 0.2 mg of GST-Afb in 2 mL of neutral PBS. The mixture was stirred for 30 min at 4 °C and then centrifuged at 3220*g* using an Eppendorf Centrifuge 5415R to remove unreacted free proteins. The obtained Col-Afb-M808 particles were washed with water and re-dispersed in PBS.

Cell culture

SK-BR-3, 4T1, and RAW 264.7 cells were purchased from Korean cell line bank (Korea). SK-BR-3 cells were cultured in DMEM media (Invitrogen); 4T1 and RAW 264.7 cells were cultured in RPMI media (Invitrogen), at 37 °C in a humidified incubator with 5% CO_2. Both media were supplemented with 10% FBS (USA) and 1% penicillin/streptomycin (Life Technologies).

Cellular uptake

In an 8-well chambered cover-glass (Lab Tek II, Thermo Scientific), SK-BR-3 cells were seeded at a density of 4×10^4 cells per well and cultured for 24 h with 10% FBS. Cells were then incubated with Col-Afb-M808s that were preloaded with a DiI dye (20 μg mL^{-1}) for 6 h, after which cellular uptake of particles was detected using confocal fluorescence imaging with a multiphoton LSM780 confocal microscope. Cells were collected by trypsinization and examined using BD FACSVerse flow cytometer (BD Biosciences, USA).

Cytotoxicity assay

In a 96-well plate, cells were seeded at a density of 5×10^3 cells per well for 24 h and treated with various samples (MOF-808@CPT, Col-Afb-M808@CPT). After another 24 h incubation, the cells were treated with 3(4,5-dimethyl-thyzoyl-2-yl) 2,5 diphenyltetrazolium bromide (MTT). Absorbance of each cell sample was then measured by using an ELISA plate reader (λ = 570 nm; n = 3). For estimation of the cell survival rate, the sample absorbance was transformed to a percentage value with respect to the absorbance of a control cell sample. Cell live-death images were confirmed through Confocal Laser Scanning Microscopy (CLSM). Live/death assessments were conducted on 4T1 cells subsequent to a 24-hour treatment, wherein IR-780 loaded samples, and resultant images were quantified.

In vivo and *ex vivo* imaging

All animal procedures were performed in accordance with the Guidelines for Care and Use of Laboratory Animals of UNIST and approved by the Institutional Animal Care and Use Committee of UNIST (UNISTIACUC-21-02). 4T1 cells were injected into the right flank of BALB/c nude female mice (Orient bio, Korea) to generate a tumor xenograft model, and the tumor was grown to a size of ~150 mm^3. The tumor-bearing mice (n = 3) were intravenously injected with 30 μg of IR-780-loaded particles that were dispersed in 100 μL of PBS buffer (pH 7.4), and their fluorescence images were acquired at various time points (0, 2, 4, 8, 24 h) using an *in vivo* optical imaging system (Bruker Xtreme model) (λ_{ex} = 630 nm; λ_{em} = 700 nm). The biodistribution of each sample was evaluated by *ex vivo* imaging from the tumor and organs extracted from the mice 24 h post-injection.

Tumor growth inhibition

To create a tumor xenograft model, 4T1 cells (1×10^6 cells) were injected into the right flank area of BALB/c nude female mice. When the tumor was grown to the volume of ~100 mm^3, IR-780 loaded MOF-808 and Col-Afb-M808s were intravenously injected to the mice (IR-780 concentration = 1.5 mg kg^{-1}; n = 5). The particle-injected mice were then treated with light (λ = 808 nm) for 3 min on the next day. This treatment with particles and light was repeated every third day and the tumor volume and body weight were measured for three weeks.

Statistical analysis

Statistical significance of difference between two groups was determined by obtaining a *P*-value in Excel *via* Student's two-tailed *t*-test. The results were expressed as the average value ± standard deviation by using all of the acquired data values. For cell viability, the raw data were processed as described above. The sample size (n) was varied and at least three.

Result & discussion

Preparation of protein–MOF complex

The nano-sized MOF-808 particles were prepared according to a reported procedure with slight modification (Fig. 2A).[14,34] Their spherical shape, approximately 50 nm in size, was imaged by scanning electron microscope (SEM) (ESI Fig. S1A†). N_2 adsorption analysis revealed a Brunauer–Emmett–Teller surface area of ~1912 m^2 g^{-1} and a pore size of ~2.0 nm (ESI Fig. S1B and S1C†). In a previous study of ours,[15] proteins were shown to be firmly grafted onto the surface of MOF particles without the need for chemical attachment. Building on this, we sought to develop an effective therapeutic nanosystem using an ECM-degradable enzyme. Two types of functional proteins were used: one to target membrane recep-

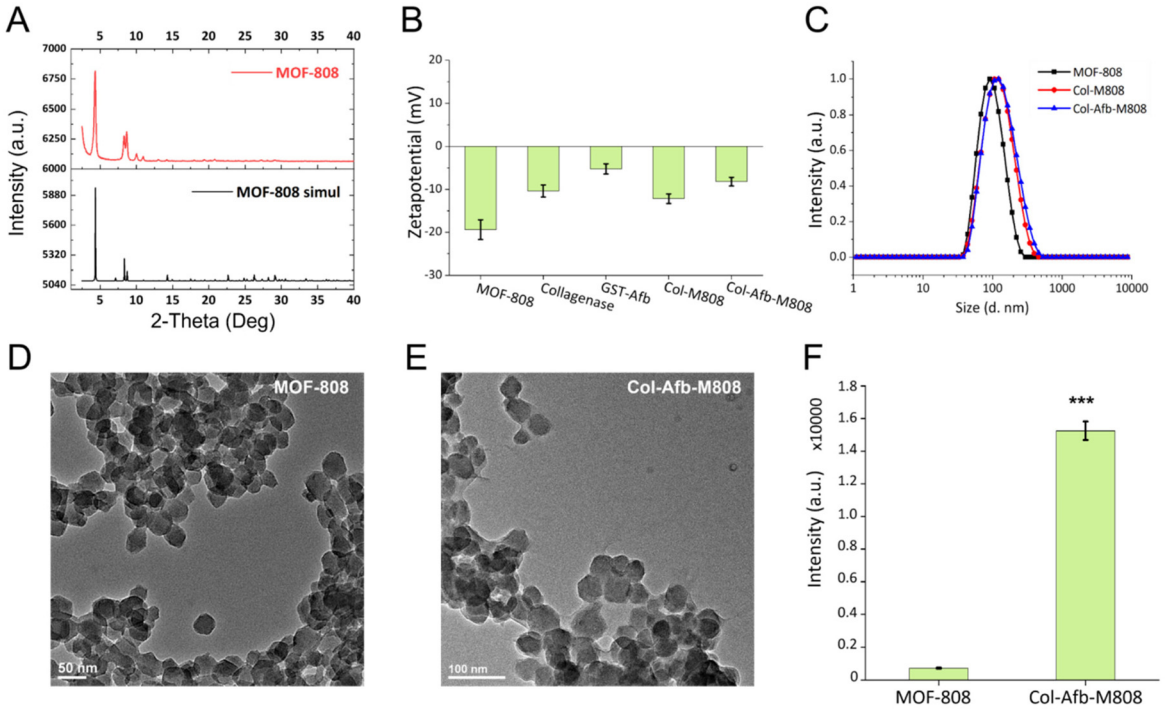

Fig. 2 Preparation of multifunctional protein–MOF complex. (A) PXRD pattern of MOF-808 particle (B) Zetapotential analysis of MOF-808, collagenous, GST-Afb, Col-M808, and Col-Afb-M808. (C) Dynamic light scattering (DLS) analysis of MOF-808, Col-M808, and Col-Afb-M808. TEM analysis of (D) MOF-808 and (F) Col-Afb-M808 (scale bar = 50, 100 nm). (F) Collagen degradation assay of MOF-808, and Col-Afb-M808 (***P < 0.001 as obtained using Student's t-test). All bar graphs indicate mean ± standard deviation (SDs) of three experimental replicates (n = 3).

tors such as HER2 or EGFR, which are overexpressed in various types of cancer, and another to degrade ECM layer found in solid tumors.[25] MOF-808 particles coated with GST-fused HER2 or EGFR-Afb proteins (GST-Afb), and collagenase were prepared using the supramolecule conjugation in neutral (pH 7.4) phosphate buffered saline (PBS). The bicinchoninic acid (BCA) assay estimated that the amount of surface-conjugated protein was similar for both collagenases-modified MOF-808 (Col-M808) (*i.e.*, ~148 μg mL^{-1}) and collagenase-GST-Afb modified MOF-808 (Col-Afb-M808) (*i.e.*, ~155 μg mL^{-1}) (ESI Fig. S2A†). Additionally, after conjugation, the surface charge of MOF-808, which was −19.1 ± 2.3 mV, became similar to the charges of the proteins: collagenase (−10.4 ± 1.4 mV) and GST-Afb (−5.23 ± 1.1 mV). Specifically, the charges were −11.2 ± 1.1 mV for Col-M808 and −7.28 ± 1 mV for Col-Afb-M808 (Fig. 2B). Furthermore, the hydrodynamic diameter of MOF-808, initially 90 ± 10 nm, increased with each protein coating step: 110 ± 10 nm for Col-M808 and 120 ± 20 nm for Col-Afb-M808 (Fig. 2C and ESI Fig. S2B†). Transmission electron microscopy (TEM) images of each particle type indicated that there was no significant deformation of the particles after protein modification (Fig. 2D, E and ESI Fig. S3C–E†). We subsequently assessed the enzymatic activity of collagenase using collagen degradation assay. The equal amounts of each sample (MOF-808, and Col-Afb-M808) were treated with a matrix of dye-quenched (DQ)-gelatin peptide conjugated with fluorescein and then monitored the intensity of released fluorescein (λ_{max} = 515 nm). Compared to the negative control (MOF-808), the multifunctional protein-grafted MOF particles (Col-Afb-M808) demonstrated significant degradation activity (Fig. 2F). Interestingly, the Col-Afb-M808 exhibited activity comparable to the solely collagen-grafted system (Col-M808) (ESI Fig. S3B†). This suggests that proteins with targeting capabilities can be incorporated without significantly compromising ECM degradation ability.

Shield effect of the multifunctional protein layer

To ensure the efficacy of MOF particles for therapeutic applications, it is imperative to prevent protein adhesion on their surfaces. This adhesion leads to the formation of a protein corona in biological environments.[16] The protein corona hampers the surface functionalities of MOF particles, including their ability to act as targeted delivery vehicles.[17–19] Moreover, when exposed to the immune system, such as the mononuclear phagocyte system (MPS),[20] particles with a protein corona can elicit undesirable immune responses,[21] resulting in potential side effects. Notably, since defect or unsaturated sites of MOF particles interact with the carboxylate groups of biological proteins at the interfaces,[28–32] the protein corona formation process could be expedited.[17] Therefore, proper regulation of defect or unsaturated sites that are present on the surface of MOF particles is necessary. For this surface regulation, we created an artificial protein corona by pre-coating with multifunctional proteins that can block

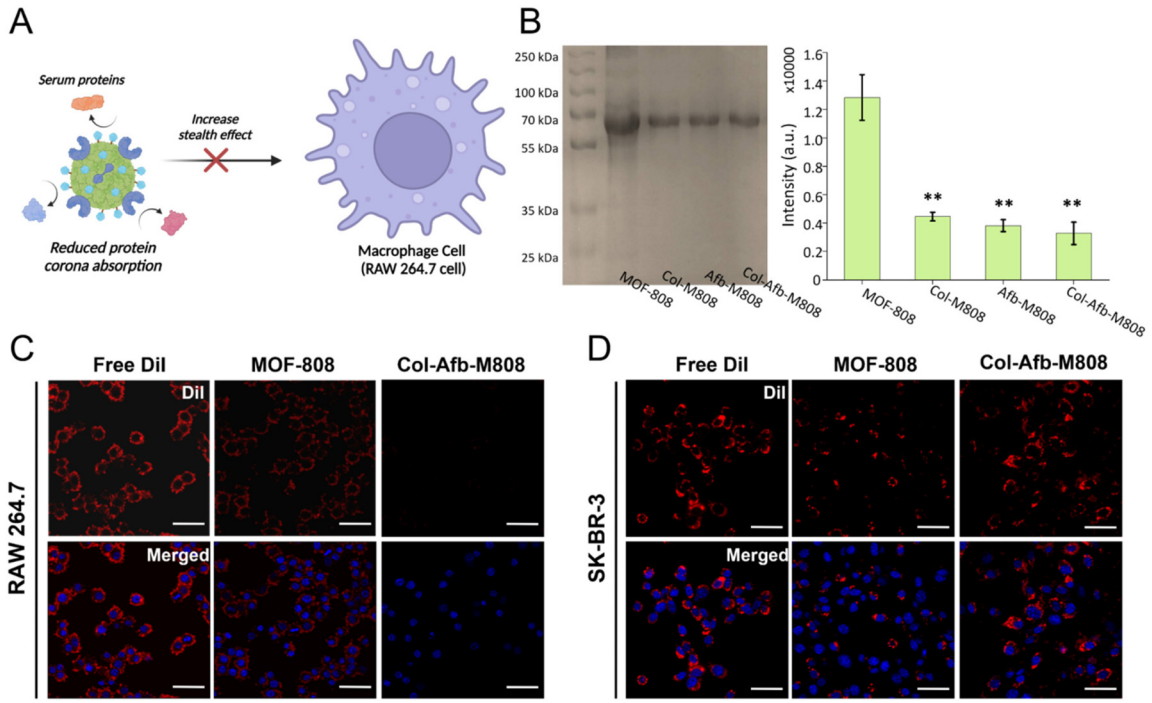

Fig. 3 Shield effect of the multifunctional protein pre-coated layer. (A) Schematic depiction of the multifunctional protein-coated MOF-808 particles that can reduce the adhesion of biomolecule proteins and, thereby, avoid immune cell (RAW 264.7) response. (B) Gel electrophoresis of MOF particles after 1 h incubation with 50% serum solutions and the resulting band intensities of MOF-808-adsorbed serum proteins (**P < 0.01 as obtained using Student's t-test; n = 3). Fluorescence microscopic images of DiI-loaded MOF particles (MOF-808 and Col-Afb-M808) after 6 h incubation with (C) RAW-264.7 and (D) SK-BR-3 (scale bar = 10 μm, red: DiI, Blue: DAPI). All bar graphs indicate mean ± standard deviation (SDs) of three experimental replicates (n = 3).

these sites before they encounter biomolecules (Fig. 3A). The degree of serum protein adsorption on the protein pre-coated MOF-808 particles (Col-M808, Afb-M808, and Col-Afb-M808) was analysed with gel electrophoresis after incubating in 50% serum media at 37 °C for 1 h and subsequent purification by centrifugation. As shown in Fig. 3B, the intense serum protein band for the pristine MOF-808 particles indicates a significant amount of serum proteins adsorbed on the surface of pristine MOF-808 particles. Following serum treatment, there was a marginal increase observed in the dimensions of Col-Afb-M808 (ESI Fig. S4†), whereas the intensity of the serum protein band exhibited a reduction of approximately 3.8-fold relative to the pristine MOF-808 particles. This demonstrates that the shield effect of the pre-coated protein layer on the surface of MOF-808 particles minimized the formation of a protein corona. To further investigate the shield effect of the pre-coated multifunctional protein layer, we tested the uptake of DiI-loaded MOF-808 and Col-Afb-M808 particles by an immune cell through a cellular uptake experiment. DiI dye-loaded MOF particles (MOF-808 and Col-Afb-M808) were prepared and then incubated for 6 h with the macrophage cell line, RAW 264.7. Confocal microscopic images show that the dye-loaded MOF-808 particles exhibit strong DiI fluorescence in the RAW 264.7 cells. However, fluorescence was barely detected in the dye-loaded Col-Afb-M808 particles. In contrast, after 6 h incubation with the HER2-receptor overexpressed cancer cell line, SK-BR-3, the fluorescence was most pronounced in the dye-loaded Col-Afb-M808 particles. Additional flow cytometry analyses were conducted to quantitatively assess these observed trends (ESI Fig. S5†). This suggests both the shield effect and the cell-specific capability of the multifunctional protein layer on the Col-Afb-M808 particles.

Multifunctional protein–MOF complex for overcoming the ECM

Based on previous results, we extended the function of the multifunctional protein layer, giving it the capability to overcome the TME. As discussed earlier, the ECM, which maintains the structure of solid tumors, hinders DDS from achieving deep tissue penetration (Fig. 4A). To address this, we incorporated collagenase into the multifunctional protein layer to degrade the collagen found in the ECM. As a result, the protein pre-coated MOF-808 particles (Col-Afb-M808) were able to achieve deep tissue penetration in a 3D multicellular spheroid model of SK-BR-3. As depicted in Fig. 4B, the DiI loaded MOF-808 particles were mostly localized on the surface of the TME structure, while the Col-Afb-M808 particles (loaded with DiI) penetrated much deeper. This trend became even more pronounced as the depth of the 3D multicellular spheroid model increased (Fig. 4B). These findings highlight the significant value of the multifunctional protein layer on Col-Afb-M808, achieving both cell-specific targeted delivery and deep tissue penetration. To assess their therapeutic efficacy, we

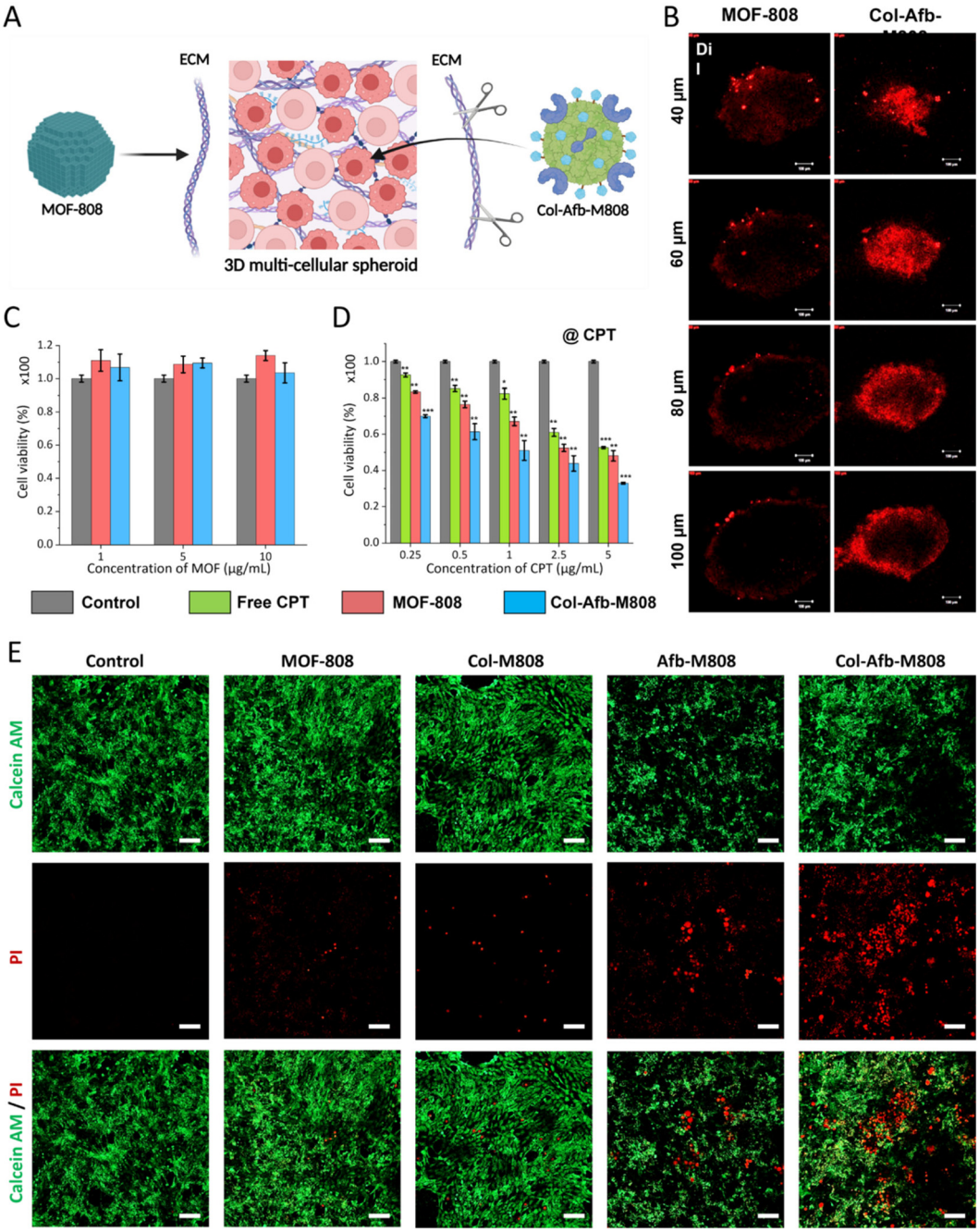

Fig. 4 Overcoming ECM for deep tissue penetration. (A) Schematic depiction of multifunctional protein-coated MOF-808 particles (C–H-M808) capable of degrading ECM in the TME to achieve deep tissue penetration. (B) Fluorescence microscopic images of DiI-loaded MOF particles (MOF-808 and Col-Afb-M808) post-incubation with the 3D multicellular spheroid cancer model, SK-BR-3 (scale bar = 100 μm; λ_{max} = 640 nm). Cytotoxicity analysis of (C) CPT-free and (D) CPT-loaded MOF particles (MOF-808 and Col-Afb-M808) on SK-BR-3 cells (n = 3) (*P < 0.05, **P < 0.01, ***P < 0.001 as obtained using Student's t-test). (E) Live-dead cell assay of 4T1 cells were irradiated with light after being treated with IR-780 loaded MOF-808, Col-M808, Afb-M808, and Col-Afb-M808 respectively (λ_{max} = 808 nm, scale bar = 100 μm). All bar graphs indicate mean ± standard deviation (SDs) of three experimental replicates (n = 3).

encapsulated an antitumor drug camptothecin (CPT) into the MOF particles before coating their surface with proteins (loading capacity = ~83 wt%, ESI Fig. S6†) and then evaluated their anticancer effect. In the absence of the drug, MOF particles (MOF-808 and Col-Afb-M808) showed no toxicity (cell survival rate close to = ~100%). However, with the drug incorporated (@CPT), cytotoxicity peaked for Col-Afb-M808, with a cell survival rate dropping to ~30%. Moreover, to validate the synergistic efficacy of the dual functional proteins on the nanoparticle surface, a photosynthesizer (IR-780) was encapsulated

within the nanoparticles, and each protein (GST-Afb and Collagenase) was either individually (Afb-M808 or Col-M808) attached or co-attached simultaneously (Col-Afb-M808). Then, the nanoparticles coated with each protein were subjected to treatment with 4T1 cells overexpressed of the EGFR receptor. After 3 h-incubation, the media was washed, and the cell was exposed to NIR laser irradiation (λ_{max} = 808 nm) for 2 min. Subsequently, cell viability was assessed using a live-dead cell

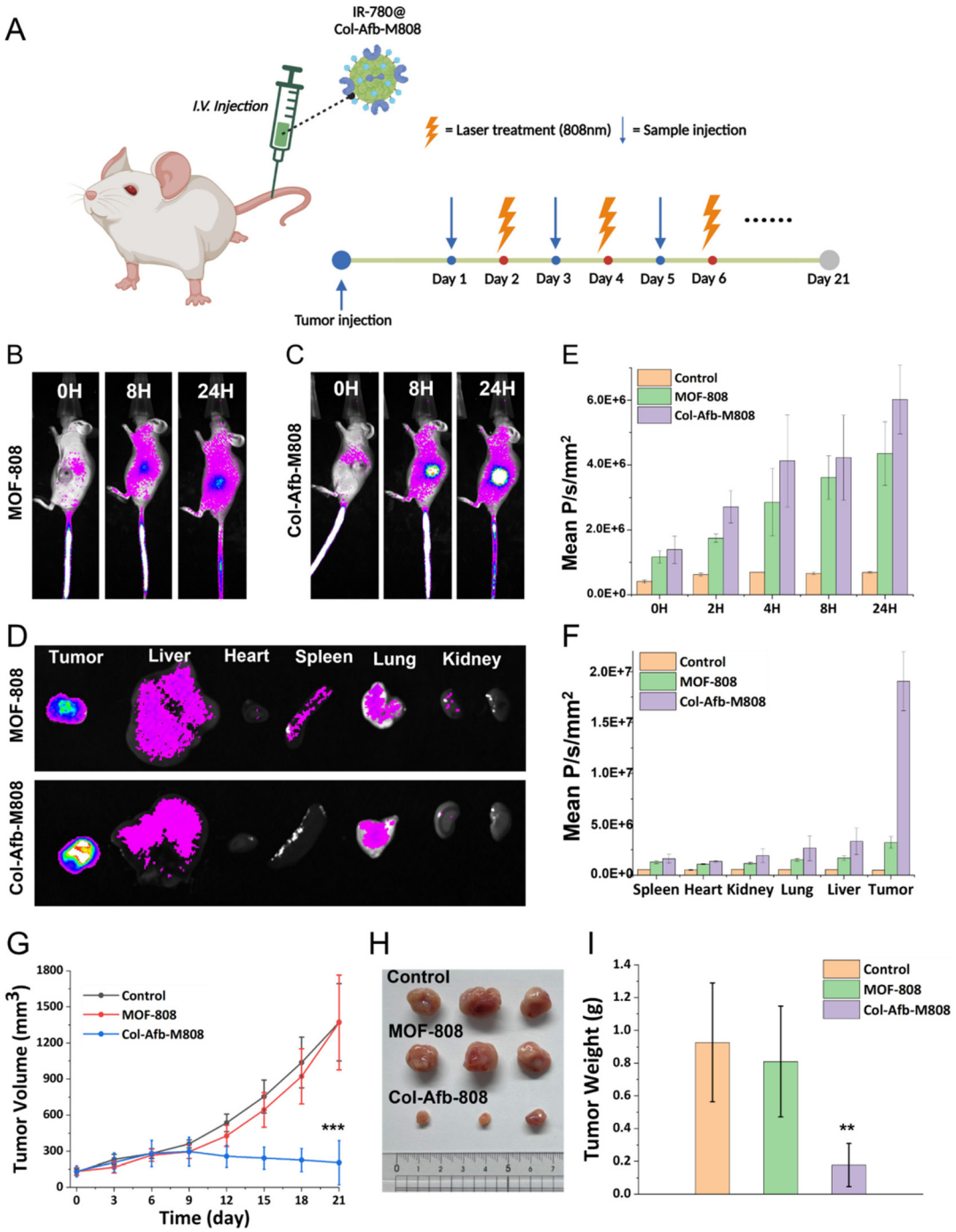

Fig. 5 *In vivo* efficacy of Col-Afb-M808. (A) Schematic illustration of the intravenous Col-Afb-M808 injection into the 4T1 tumor-bearing mice for targeted tumor accumulation and light irradiation (n = 5). Fluorescence emission from the 4T1-bearing mice (side) that were intravenously injected with IR-780 loaded (B) MOF-808, and (C) Col-Afb-M808 (n = 3). (D) Fluorescence image of the organs and tumors collected at 24 h after the material injection into the mice. Fluorescence intensities detected for 24 h in (E) the tumor site during *in vivo* fluorescence imaging (F) and the organs and tumor in the *ex vivo* image (λ_{ex} = 630 nm; λ_{em} = 700 nm). (G) Changes in tumor volume for three weeks. (H) Tumors extracted from the mice after treatment with different materials and (I) their weights. ***P < 0.001 as obtained using Student's t-test.

assay kit (Fig. 4E). As a result, non-target-directed Col-M808 demonstrated comparable levels of cell death to MOF-808. The target-specific Afb-M808 exhibited heightened cytotoxicity in comparison to the preceding two samples; however, it did not attain the level of efficacy observed in Col-Afb-M808, incorporating both functional proteins. These findings unequivocally illustrate the maximization of the synergistic effect when both functional entities are concomitantly present.

Therapeutic efficacy of Col-Afb-M808

Finally, we expanded our investigation into the biodistribution and therapeutic efficacy of Col-Afb-M808 using a tumor xenograft model (Fig. 5A). Tumor targeting was assessed by intravenously administering IR-780-loaded Col-Afb-M808 particles to 4T1 tumor-bearing nude mice (n = 3 mice per group). Enhanced fluorescence emission at tumor sites indicated a significant increase in IR-780 accumulation, compared to the case when treated with PBS or IR-780 loaded MOF-808 particles (Fig. 5B, ESI Fig. S7 and S8†). At 24 hours post-administration, major organs and tumors were excised, and their fluorescence images confirmed selective accumulation of Col-Afb-M808 in tumors (Fig. 5C).

Subsequently, the anti-tumor efficacy was evaluated using the mice that were treated with PBS, IR loaded MOF-808, or Col-Afb-M808 *via* i.v. injection when the tumor volume was ~150 mm^3. In addition, tumors were irradiated with light (λ_{max} = 808 nm) for three minutes after 24 hours post injection, and this treatment was repeated for three weeks (Fig. 5A). Notably, Col-Afb-M808 treatment led to substantial reduction of the tumor volume by day 21, compared to the control groups (~85%, Fig. 5G). Correspondingly, tumor mass was significantly reduced as shown in Fig. 5H and I. Additionally, the stability of body weight throughout the treatment period suggests the biocompatibility of our nanoparticle-based delivery system (ESI Fig. S9†).

Conclusions

In this study, we successfully developed a DDS system precoated with multifunctional protein, utilizing MOF-808 nanoparticles. This system involved coating these nanoparticles with both targetable GST-Afb and an ECM degradable enzyme, collagenase. Remarkably, the interaction between the protein and MOF particle surface was achieved through supramolecular conjugation. This was accomplished by simple mixing, eliminating the need for chemical fixation. Our investigations demonstrated the exceptional stability of the pre-coated multifunctional protein layer on the particle surface. This layer minimized non-specific protein adsorption and enabled the degradation of the ECM barrier present in the 3D structure of tumor tissue. As a result, our system exhibited enhanced penetration into deep tissue regions, facilitating effective target-specific delivery both *in vitro* and *in vivo*. These findings shed light on strategies to enhance the targeting and penetration capabilities of multiprotein MOF-based delivery systems.

Data availability

The data supporting this article have been included as part of the ESI.†

Author contributions

J.-H. R. supervised this study and wrote the manuscript. J. Y. O., M.-S. S., and A. K. B. have equally contributed, designed, carried out and analysed data from most of the experiments, and wrote the manuscript with input from all co-authors. M.-S. S. did *in vivo* experiment. J. S., D. K., and H. W. O. helped cell experiments. M. S. L. was editing overall manuscript. E. C. helped preparation of a manuscript. All authors discussed the results and commented on the manuscript.

Conflicts of interest

There are no conflicts to declare.

Acknowledgements

This work was supported by National Research Foundation of Korea (NRF) grants funded by the Korean Government (MSIT) (2022R1A2C2005339, RS-2023-00208386, RS-2023-00281553, RS-2023-00255698, 2020M3A9D8038192, 2022R1A6A3A01085939).

References

1 Y. Bai, Y. Dou, L.-H. Xie, W. Rutledge, J.-R. Li and H.-C. Zhou, *Chem. Soc. Rev.*, 2016, **45**, 2327–2367.
2 J. Yang and Y.-W. Yang, *View*, 2020, **1**, e20.
3 C. Orellana-Tavra, E. F. Baxter, T. Tian, T. D. Bennett, N. K. H. Slater, A. K. Cheetham and D. Fairen-Jimenez, *Chem. Commun.*, 2015, **51**, 13878–13881.
4 J. W. M. Osterrieth and D. Fairen-Jimenez, *Biotechnol. J.*, 2021, **16**, 2000005.
5 B. Li, H.-M. Wen, Y. Cui, W. Zhou, G. Qian and B. Chen, *Adv. Mater.*, 2016, **28**, 8819–8860.
6 Q.-L. Zhu and Q. Xu, *Chem. Soc. Rev.*, 2014, **43**, 5468–5512.
7 A. Bétard and R. A. Fischer, *Chem. Rev.*, 2012, **112**, 1055–1083.
8 M. Al Sharabati, R. Sabouni and G. A. Husseini, *Nanomaterials*, 2022, **12**, 277.
9 I. Abánades Lázaro, S. Haddad, J. M. Rodrigo-Muñoz, R. J. Marshall, B. Sastre, V. del Pozo, D. Fairen-Jimenez and R. S. Forgan, *ACS Appl. Mater. Interfaces*, 2018, **10**, 31146–31157.
10 M. Pander, A. Żelichowska and W. Bury, *Polyhedron*, 2018, **156**, 131–137.
11 M. Kim and S. M. Cohen, *CrystEngComm*, 2012, **14**, 4096–4104.
12 H. Furukawa, F. Gándara, Y.-B. Zhang, J. Jiang, W. L. Queen, M. R. Hudson and O. M. Yaghi, *J. Am. Chem. Soc.*, 2014, **136**, 4369–4381.

13 R. J. Marshall and R. S. Forgan, *Eur. J. Inorg. Chem.*, 2016, **2016**, 4310–4331.
14 J. Jiang, F. Gándara, Y.-B. Zhang, K. Na, O. M. Yaghi and W. G. Klemperer, *J. Am. Chem. Soc.*, 2014, **136**, 12844–12847.
15 J. Y. Oh, E. Choi, B. Jana, E. M. Go, E. Jin, S. Jin, J. Lee, J.-h. Bae, G. Yang, S. K. Kwak, W. Choe and J.-H. Ryu, *Small*, 2023, **19**, 2300218.
16 J. Y. Oh, H. S. Kim, L. Palanikumar, E. M. Go, B. Jana, S. A. Park, H. Y. Kim, K. Kim, J. K. Seo, S. K. Kwak, C. Kim, S. Kang and J.-H. Ryu, *Nat. Commun.*, 2018, **9**, 4548.
17 J. Y. Oh, E.-K. An, B. Jana, H. Kim, S. Jin, G. Yang, J. Kim, E. Choi, J.-O. Jin and J.-H. Ryu, *Chem. Eng. J.*, 2023, **470**, 144357.
18 A. Zimpel, N. Al Danaf, B. Steinborn, J. Kuhn, M. Höhn, T. Bauer, P. Hirschle, W. Schrimpf, H. Engelke, E. Wagner, M. Barz, D. C. Lamb, U. Lächelt and S. Wuttke, *ACS Nano*, 2019, **13**, 3884–3895.
19 P. C. Ke, S. Lin, W. J. Parak, T. P. Davis and F. Caruso, *ACS Nano*, 2017, **11**, 11773–11776.
20 M. V. Zyuzin, Y. Yan, R. Hartmann, K. T. Gause, M. Nazarenus, J. Cui, F. Caruso and W. J. Parak, *Bioconjugate Chem.*, 2017, **28**, 2062–2068.
21 A. E. Nel, L. Mädler, D. Velegol, T. Xia, E. M. V. Hoek, P. Somasundaran, F. Klaessig, V. Castranova and M. Thompson, *Nat. Mater.*, 2009, **8**, 543–557.
22 A. K. Barui, J. Y. Oh, B. Jana, C. Kim and J.-H. Ryu, *Adv. Ther.*, 2020, **3**, 1900124.
23 I. Elia and M. C. Haigis, *Nat. Metab.*, 2021, **3**, 21–32.
24 A. Tiwari, R. Trivedi and S.-Y. Lin, *J. Biomed. Sci.*, 2022, **29**, 83.
25 R. Baghban, L. Roshangar, R. Jahanban-Esfahlan, K. Seidi, A. Ebrahimi-Kalan, M. Jaymand, S. Kolahian, T. Javaheri and P. Zare, *Cell Commun. Signaling*, 2020, **18**, 59.
26 G. S. Hussey, J. L. Dziki and S. F. Badylak, *Nat. Rev. Mater.*, 2018, **3**, 159–173.
27 J. K. Mouw, G. Ou and V. M. Weaver, *Nat. Rev. Mol. Cell Biol.*, 2014, **15**, 771–785.
28 M. Hu, Z. Ling and X. Ren, *J. Biol. Eng.*, 2022, **16**, 13.
29 Y. Liu, W. Hou, L. Xia, C. Cui, S. Wan, Y. Jiang, Y. Yang, Q. Wu, L. Qiu and W. Tan, *Chem. Sci.*, 2018, **9**, 7505–7509.
30 Z. Wang, Y. Fu, Z. Kang, X. Liu, N. Chen, Q. Wang, Y. Tu, L. Wang, S. Song, D. Ling, H. Song, X. Kong and C. Fan, *J. Am. Chem. Soc.*, 2017, **139**, 15784–15791.
31 J. Park, Q. Jiang, D. Feng, L. Mao and H.-C. Zhou, *J. Am. Chem. Soc.*, 2016, **138**, 3518–3525.
32 K. Ni, T. Luo, A. Culbert, M. Kaufmann, X. Jiang and W. Lin, *J. Am. Chem. Soc.*, 2020, **142**, 12579–12584.
33 C. He, K. Lu, D. Liu and W. Lin, *J. Am. Chem. Soc.*, 2014, **136**, 5181–5184.
34 A. Sharma, J. Lim, S. Lee, S. Han, J. Seong, S. B. Baek and M. S. Lah, *Angew. Chem., Int. Ed.*, 2023, **62**, e202302376.